AD-A189 288

OFFICE OF NAVAL RESEARCH

Contract N00014-86-K-0556

Technical Report No. 65

Characterization of Redox Sates of Nickel Hydroxide Film Electrodes

by In-Situ Raman Spectroscopy

by

J. Desilvestro, D. A. Corrigan, and M. J. Weaver

Prepared for Publication

in the

Journal of Electrochemical Society

Purdue University

Department of Chemistry

West Lafayette, Indiana 47907

DTIC
ELECTE
DEC 2 9 1987
H

September 25, 1987

REPORT DOCUMENTATION PAGE

1a. REPORT SECURITY CLASSIFICATION Unclassified	1b. RESTRICTIVE MARKINGS
2a. SECURITY CLASSIFICATION AUTHORITY	3. DISTRIBUTION/AVAILABILITY OF REPORT Approved for public release and sale; its distribution is unlimited.
2b. DECLASSIFICATION/DOWNGRADING SCHEDULE	
4. PERFORMING ORGANIZATION REPORT NUMBER(S) Technical Report No. 65	5. MONITORING ORGANIZATION REPORT NUMBER(S)

6a. NAME OF PERFORMING ORGANIZATION Purdue University Department of Chemistry	6b. OFFICE SYMBOL (If applicable)	7a. NAME OF MONITORING ORGANIZATION Division of Sponsored Programs Purdue Research Foundation
6c. ADDRESS (City, State, and ZIP Code) Purdue University Department of Chemistry West Lafayette, Indiana 47907		7b. ADDRESS (City, State, and ZIP Code) Purdue University West Lafayette, Indiana 47907
8a. NAME OF FUNDING/SPONSORING ORGANIZATION Office of Naval Research	8b. OFFICE SYMBOL (If applicable)	9. PROCUREMENT INSTRUMENT IDENTIFICATION NUMBER Contract No. N00014-86-K-0556

8c. ADDRESS (City, State, and ZIP Code) 800 N. Quincy Street Arlington, VA 22217	10. SOURCE OF FUNDING NUMBERS			
	PROGRAM ELEMENT NO	PROJECT NO	TASK NO	WORK UNIT ACCESSION NO

11. TITLE (Include Security Classification)

Characterization of Redox States of Nickel Hydroxide Film Electrodes by In-Situ Raman Spectroscopy

12. PERSONAL AUTHOR(S)

J. Desilvestro, D. A. Corrigan, and M. J. Weaver

13a. TYPE OF REPORT Technical	13b. TIME COVERED FROM 10/1/86 TO 9/30/87	14. DATE OF REPORT (Year, Month, Day) September 25, 1987	15. PAGE COUNT

16. SUPPLEMENTARY NOTATION

17.	COSATI CODES		18. SUBJECT TERMS (Continue on reverse if necessary and identify by block number)
FIELD	GROUP	SUB-GROUP	in-situ, surface Raman spectroscopy, nickel hydroxide, films, electrodes, cyclic voltammetry

19. ABSTRACT (Continue on reverse if necessary and identify by block number)

Thin films of nickel hydroxide deposited on gold electrodes have been characterized in detail by in-situ surface Raman spectroscopy in conjunction with electrochemical techniques. Raman spectra were obtained for film thicknesses varying from less than one equivalent monolayer to several hundred monolayers, as determined from the faradaic charge for the cyclic voltammetric oxidation of $Ni(OH)_2$. For the thinnest films, Raman bands at 455/cm and at 480 and 560/cm were obtained for the reduced and oxidized films, respectively, using 647.1 nm excitation at roughened gold. These signals, identified with Ni-OH and Ni-O vibrations from deuterium isotope data, were diagnosed as arising from surface-enhanced Raman scattering (SERS) in view of their absence for the reduced film when using smooth gold surfaces and/or green/blue laser excitation. Raman spectra were obtained using the latter conditions for thicker oxidized films, which were consistent with resonance Raman scattering (RRS). Analysis of the dependence of the 480/560 cm^{-1} band intensities as a function of film thickness under conditions where SERS or RRS predominates enables the relative contributions of these mechanisms as well as the
(continued on back)

20. DISTRIBUTION/AVAILABILITY OF ABSTRACT ☐ UNCLASSIFIED/UNLIMITED ☒ SAME AS RPT ☐ DTIC USERS	21. ABSTRACT SECURITY CLASSIFICATION Unclassified
22a. NAME OF RESPONSIBLE INDIVIDUAL	22b. TELEPHONE (Include Area Code) | 22c. OFFICE SYMBOL

DD FORM 1473, 84 MAR
83 APR edition may be used until exhausted
All other editions are obsolete

CHARACTERIZATION OF REDOX STATES OF NICKEL HYDROXIDE FILM ELECTRODES

BY IN SITU SURFACE RAMAN SPECTROSCOPY

Johann Desilvestro, Dennis A. Corrigan[+], and Michael J. Weaver

Department of Chemistry

Purdue University

West Lafayette, Indiana 47907, U.S.A.

[+]Electrochemistry Department, General Motors Research Laboratories, Warren, Michigan 48090, U.S.A.

ABSTRACT

Thin films of nickel hydroxide deposited on gold electrodes have been characterized in detail by in-situ surface Raman spectroscopy in conjunction with electrochemical techniques. Raman spectra were obtained for film thicknesses varying from less than one equivalent monolayer to several hundred monolayers, as determined from the faradaic charge for the cyclic voltammetric oxidation of $Ni(OH)_2$. For the thinnest films, Raman bands at 455 cm^{-1} and at 480 and 560 cm^{-1} were obtained for the reduced and oxidized films, respectively, using 647.1 nm excitation at roughened gold. These signals, identified with Ni-OH and Ni-O vibrations from deuterium isotope data, were diagnosed as arising from surface-enhanced Raman scattering (SERS) in view of their absence for the reduced film when using smooth gold surfaces and/or green/blue laser excitation. Raman spectra were obtained using the latter conditions for thicker oxidized films, which were consistent with resonance Raman scattering (RRS). Analysis of the dependence of the 480/560 cm^{-1} band intensities as a function of film thickness under conditions where SERS or RRS predominates enables the relative contributions of these mechanisms as well as the influence of film absorbance to be assessed quantitatively. Raman spectra were also obtained in air and after "film aging" by potential cycling or heating. The spectral changes following the latter treatments support the evolution of a less hydrogen-bound $Ni(OH)_2$ film structure, i.e. the transformation of α- to β-$Ni(OH)_2$. By combining cyclic voltammetry with analysis of the dissolved film using atomic absorption spectroscopy, the effective oxidation state of nickel in the oxidized films is determined to be + 3.7 (± 0.04). On the basis of the spectroscopic and electrochemical measurements, the most likely structure for the oxidized film is $M(NiO_2)_3$, where M is the supporting electrolyte cation.

INTRODUCTION

Nickel oxide electrodes have long been of importance in storage battery systems (1).[*] More recently, nickel oxide films have attracted much interest as electrocatalysts for the oxidation of alcohols or amines (2) and as electrochromic devices (3). Despite this variety of applications, the structural changes accompanying the redox electrochemistry of nickel oxide films are still controversial. Of particular interest is the nature of the multiple crystalline phases formed in both the reduced and oxidized states and the valence state of the oxidized film. Although a widely held view is that the oxidized film is NiOOH (1a,1b,4), it is known that nickel oxide electrodes can be charged up to $Ni^{3.75+}$(1b,5).

The scarcity of structural information recently stimulated us to examine thin nickel oxide films on gold using surface-enhanced Raman spectroscopy (SERS) (6). This work forms a part of our recent studies on electrochemical applications of SERS at gold (7-9), including the in-situ monitoring of surface redox transformations (8). Apart from studies of adsorbates at unmodified gold electrodes, SERS has been observed for gold substrates coated with a variety of thin "SERS-inactive" overlayers, including metals such as mercury, lead, thallium (9a), platinum and palladium (9b), and various metal oxides (6,8d,9c).

In ref. 6 we established that SERS could be utilized to examine very thin (a few monolayers thick) films of $Ni(OH)_2$ formed on gold electrodes by cathodic electrodeposition, and to follow their in-situ oxidation,

---

[*] This paper commemorates the 100th anniversary of the first proposed application of the nickel oxide electrode in galvanic cells, by Dun, Hesslacher, and Desmazures (1c).

primarily from the changes in the nickel-oxygen (Ni-O) stretching frequencies. This paper presents a more detailed characterization of nickel oxide films on noble metal substrates by means of electrochemical and in-situ surface Raman spectroscopic techniques. Emphasis is placed on spectroscopic as well as electrochemical measurements as a function of film thickness in order to clearly deduce conditions for which surface-enhanced Raman, resonance Raman, and/or normal Raman scattering mechanisms contribute predominantly to the observed Raman signals. These results provide new information on the structure of the potential-dependent redox states of nickel oxide for a wide range of film thicknesses.

EXPERIMENTAL

Potassium hydroxide (ultrapure) and β-Ni(OH)$_2$ powder were obtained from Alfa Products. The different Ni(OH)$_2$ samples were analyzed by X-ray analysis and identified as either in the α- or β-form (5a,c). Other chemicals were reagent grade and used as supplied. Water was purified by means of a "Milli-Q" system (Millipore Corp.).

The gold and platinum electrodes (Pine Instruments Co.) consisted of a 4 mm gold disk sealed into a 12 mm diameter Teflon sheath. The electrochemical roughening procedure to generate SERS activity on gold has been described previously (8a,8d). After activation the electrode was thoroughly rinsed with water and transferred to the solution of interest. The nickel electrode was a 0.1 mm thick nickel foil (99.8% Ni).

Electrochemical and surface Raman measurements were performed in two-compartment cells, using gold counter electrodes. Electrode potentials or currents were adjusted by a PAR Model 173/179 potentiostat-galvanostat in conjunction with a computer-controlled interface or a PAR Model 175 Universal Programmer. All potentials were measured and are quoted versus

the saturated calomel electrode (SCE).

Details of the laser Raman system used for the electrochemical SER measurements are chiefly as given in ref. 10. Raman excitation was provided by a Spectra Physics Model 165 Kr^+ laser (wavelength $\lambda = 647.1$ or 676.4 nm) or a Model 165 Ar^+ laser (457.9, 472.7, 476.5, 488.0, or 514.5 nm) with s-polarized light (i.e. perpendicular to the plane of incidence) at the planar samples. The angle between the incident light and the flat samples or cell windows was adjusted to 30°. The scattered light was collected orthogonal to the incident light with a SPEX Model 1403 scanning spectrometer. With the exception of the SER experiments, a scrambler was used to depolarize the scattered Raman light. Powdered $Ni(OH)_2$ samples were diluted with 75 weight percent KBr, pressed, and the so-obtained 7 mm diameter disks were rotated while recording Raman spectra in order to minimize heating of the colored samples.

Atomic absorption measurements for assaying nickel were performed with a Perkin Elmer Model 2380 spectrometer at a wavelength of 232.0 nm and a 0.2 mm slit width. Calibration was achieved using a 5.0 ppm standard solution of Ni^{2+}.

Excitation profiles (i.e. Raman scattering intensity versus laser wavelength) were obtained by correcting the measured integrated Raman intensities I_i, I_j corresponding to a pair of wavelengths λ_i, λ_j for the variable monochromator and photomultiplier response by using the following formula:

$$I'_i/I'_j = (\lambda_j/\lambda_i)^4 \cdot (I_i I_j^r / I_j I_i^r) \tag{1}$$

The calibration was performed with a suitable reference sample (CCl_4,

460 cm^{-1} band) and assumed that the band intensity, I^r, is proportional to λ^{-4}, as expected for normal Raman scattering.

RESULTS

Ni(OH)$_2$ film formation and electrochemical characterization

The nickel oxide films were prepared by cathodic galvanostatic precipitation as Ni(OH)$_2$ from Ni(NO$_3$)$_2$ solutions (1,5a,5d,11). In spite of this earlier work, the electrodeposition mechanism is insufficiently characterized. We therefore conducted a brief examination of this process, as regards the influence of the electrolyte anion and the coulombic deposition efficiency.

Figure 1 compares cathodic galvanostatic potential-time curves, at 0.8 mA cm^{-2}, for Ni(OH)$_2$ deposition onto gold from 0.01 $\underline{M}$ Ni(NO$_3$)$_2$, Ni(ClO$_4$)$_2$, and NiSO$_4$ solutions, and subsequent open-circuit potential decay. It is seen that the presence of nitrate anions induce substantially different potential-time behavior, yielding lower cathodic overpotentials and markedly more rapid open-circuit potential decay than with ClO$_4^-$ or SO$_4^{2-}$. The addition of nitrate anions to the Ni(ClO$_4$)$_2$ or NiSO$_4$ solutions yielded comparable electrochemical behavior (dashed trace in Fig. 1) to that for the Ni(NO$_3$)$_2$ solutions. The form of the potential-time curves was very similar on the electrochemically roughened (i.e. SERS-active) gold as for "smooth" (i.e. mechanically polished) samples. Alterations in the cathodic current (8 μA cm^{-2} to 8 mA cm^{-2}) as well as the deposition time were employed so to produce films of widely varying thickness.

The Ni(OH)$_2$ film electrodes were then transferred to 1 $\underline{M}$ KOH for characterization by anodic-cathodic cyclic voltammetry. The faradaic charge densities contained under the Ni(II) oxidation wave, q_f^a, and for the subsequent reduction, q_f^c, provide a measure of the film thickness (Fig. 2;

see also Fig. 1 in ref. 6). Films on gold with thicknesses corresponding to q_f^a ~ 0.02 to 20 mC cm^{-2} were examined here; this corresponds to roughly 0.1 to 100 equivalent monolayers of $Ni(OH)_2$.[*] The cyclic voltammogram (solid trace) shown in Fig. 2 corresponds to a relatively thin film, ca. 5, monolayers. Although $q_f^a > q_f^c$ at low scan rates, for faster scans (~ 50 mV s^{-1}) and/or for thicker films, $q_f^a \approx q_f^c$. Continued potential cycling leads eventually to slight positive shifts in both the anodic and cathodic peak potentials (compare solid and dashed curves in Fig. 2). A similar transformation, although at a smaller rate, was observed after soaking the film in 1 $\underline{M}$ KOH under open-circuit conditions or by holding the potential at -0.1 V or 0.45 V. Heating in 5 $\underline{M}$ KOH at 60°C for 1-3 hours resulted in voltammograms with much broader anodic and cathodic features, centered at 0.45 and 0.27 V, respectively, for a sweep rate of 20 mV s^{-1}. Slightly different voltammograms were obtained for thicker films, as shown by the dotted curve in Fig. 2 which corresponds to q_f ~ 19 mC cm^{-2}.

In order to evaluate the efficiency and also mechanism of the $Ni(OH)_2$ film deposition process, it is useful to compare the voltammetric charge density required for film oxidation, q_f^a, with the corresponding faradaic charge density, q_g, passed during the galvanostatic deposition process. Figure 3 shows resulting plots of q_f versus q_g for various film thicknesses prepared using three solutions, 0.01 $\underline{M}$ $Ni(NO_3)_2$ (circles), $Ni(ClO_4)_2$ (squares), and $NiSO_4$ (triangles). The two straight lines shown correspond to q_f/q_g ratios of 1 and 0.5. Although there is considerable scatter it is seen that most of the points referring to deposition from $Ni(NO_3)_2$ fall

---

[*]From crystallographic data for "α-Ni(OH)$_2$", $3Ni(OH)_2 \cdot 2H_2O$ (5c), we obtain 1.06×10^{-9} mol cm^{-2} of Ni per monolayer. Assuming that 1.7 e$^-$ are transferred during $Ni(OH)_2$ electrooxidation (vide infra) this corresponds to about 0.17 mC cm^{-2} monolayer^{-1}. Allowing for electrode roughness, this figure is approximated here as 0.2 mC cm^{-2} monolayer^{-1}.

between these two lines, whereas substantially smaller deposition efficiencies (i.e. smaller q_f/q_g ratios) are found using the other two solutions. This further implicates the specific role played by NO_3^- during the electrodeposition process.

As noted above, there is strong evidence that the electrooxidation of $Ni(OH)_2$ yields a nickel valence state substantially above +3, probably around +3.7 (1b,5). To check this for the relatively thin films studied here, we determined the effective number of electrons, n, required for the voltammetric oxidation of $Ni(OH)_2$. This was achieved by assaying the quantity of nickel present in a film yielding a faradaic oxidation charge, Q_f^a, for a given electrode area. The number of moles of nickel, m, were obtained by means of atomic absorption spectroscopy after dissolving the film in 1 $\underline{M}$ HCl, enabling n to be obtained from $n = Q_f^a/Fm$. Three replicate measurements for two film thicknesses, corresponding to $q_f^a = 3$ and 9 mC cm^{-2}, yielded $n = 1.7 \pm 0.04$. We therefore deduce that the valence state of nickel in the oxidized film is indeed about 3.7, even for very thin films.

Raman Spectroscopy of $Ni(OH)_2$ Films

Surface Raman spectra of the nickel oxide films were examined over a wide range of conditions, primarily in in situ electrochemical environments, in order to distinguish between the various scattering mechanisms that can contribute to the observed signals as well as to gain information on the film structural properties as a function of thickness and redox state. We will first consider spectral data for the unoxidized $Ni(OH)_2$ films.

As noted previously (6), easily detectable Raman features were obtained using 647.1 nm excitation on electrochemically roughened (i.e.

SERS-active) gold, even for film thicknesses below one equivalent monolayer. A typical spectrum recorded for such a film in air using a backscattering geometry is shown in Fig. 4a; a strong band around 455 cm^{-1} is obtained, with weaker and broader features around 3525 and 3670 cm^{-1}. Transferring the sample to 1 $\underline{M}$ KOH and applying a potential of -0.2 V yielded practically the same spectrum in the low-frequency region, albeit with a lower intensity due to reflection losses in the electrochemical cell. The high-frequency region, however, was obscured by a broad Raman band around 3000 - 3750 cm^{-1} due to the background electrolyte. No clearcut dependence of the 455 cm^{-1} band intensity on the film thickness was obtained. Surprisingly, the marked changes noted above in the electrochemical redox behavior of the $Ni(OH)_2$ films seen upon potential cycling or heating in 5$\underline{M}$ KOH (60°C for 3 hrs) were not paralleled by significant changes in the SER spectra, either in solution or in air. As noted in ref. 6, the 455 cm^{-1} peak shifted to 446 cm^{-1} using alkaline D_2O rather than H_2O solutions.

It is well known that SERS on gold is obtained only for roughened surfaces using laser wavelengths above 580 nm (12). Therefore a clear diagnosis of these Raman signals as originating from SERS is obtained by the observed absence of detectable signals when 488 or 514.5 nm, rather than 647.1 nm, excitation was employed (6). Also, no Raman signals could be detected for $Ni(OH)_2$ films when smooth gold or nickel surfaces were used as the substrate, even for films up to 2000 equivalent monolayers. Thicker films could not readily be studied since they showed a poor mechanical adherence to the substrate. Nevertheless, green $Ni(OH)_2$ powder collected from $Ni(OH)_2$ deposits on nickel when pressed into a KBr pellet yielded detectable Raman spectra. These samples were identified as α-$Ni(OH)_2$ by X-

ray diffraction. In Fig. 4c we show, to our knowledge for the first time, a Ramann of this material, having a band at 465 cm^{-1} and weak features around 351, 376, 528, and 3585 cm^{-1} (Fig. 4c).

Relatively thick $Ni(OH)_2$ films ($q_f \approx 0.4$ C cm^{-2}), deposited on nickel and "aged" by immersion in water at 90°C for 3 hours, nevertheless yielded detectable Raman spectra, with weak bands at 315 and 450 cm^{-1} and a more intense peak at 3580 cm^{-1}. More intense, yet similar, spectral features were obtained using commercial β-$Ni(OH)_2$ powder, with bands at 314 and 449 cm^{-1}, with weaker features at 376 and 516 cm^{-1}, and a very intense band at 3560 cm^{-1} (Fig. 4d). Very similar Raman spectra for β-$Ni(OH)_2$ have been reported previously (13).

Raman spectroscopy of oxidized films

We have summarized previously the Raman spectral changes accompanying the potential-dependent oxidation of thin $Ni(OH)_2$ films on roughened gold, where the signals arise predominantly from SERS (6). The 455 cm^{-1} band disappears just prior to the onset of film oxidation, and a pair of new bands at 480 and 560 cm^{-1} emerges. By obtaining time-resolved spectra for a thin film (ca. 5 monolayers) during a slow anodic-cathodic cyclic voltammogram, the intensities of the latter bands were shown to be approximately proportional to the extent of oxidation (6).

In contrast to the reduced films, measurable Raman signals were obtained for oxidized films, of thicknesses $\geq$ 10 monolayers, even for smooth gold or platinum surfaces, or for blue or green laser light for which SERS will be essentially absent. Consistent with this, the spectra were unaffected by surface roughening when blue or green excitation was employed. The appearance of the 480 and 560 cm^{-1} bands under these

conditions during oxidation of thick films, however, differed significantly from the SERS thin-film behavior noted above. For example, for a relatively thick (100 monolayer) film on smooth gold, the two bands at 480 and 560 cm^{-1} appeared when the film was about 20% oxidized and the maximum band intensity was achieved at only 35% oxidation, the completion of film oxidation resulting in a slight intensity decrease.

Thick oxidized films on either gold or platinum in air also yielded only two major Raman bands at 480 and 560 cm^{-1} (Fig. 5j). In contrast to the behavior of the reduced films in air, however, no spectral features were observed between 3200 and 3800 cm^{-1}. As noted in ref. 6, no detectable ($\leq$ 1-2 cm^{-1}) shift in either the 480 or 560 cm^{-1} band frequencies were obtained when alkaline D_2O solution was used in place of H_2O. The band frequencies were also independent of the nature of the supporting electrolyte cation (Li^+, Na^+, K^+) and did not shift when the potential was increased up to 0.7 V where vigorous O_2 evolution occurred. Essentially the same Raman spectra were obtained when the $Ni(OH)_2$ layers were oxidized either electrochemically or under open-circuit conditions with 0.02 $\underline{M}$ $K_2S_2O_8$ in 1 $\underline{M}$ KOH.

The oxidized films were slowly reduced spontaneously both in air or in 1 $\underline{M}$ KOH under open circuit, as indicated by the disappearance of the 480/560 cm^{-1} doublet and in the latter case by the gradual negative drift of the electrode potential. The time period required for complete spontaneous reduction was of the order of 30 min. for films around five equivalent monolayers, and lengthened with increasing film thickness.

Dependence of Raman intensity for oxidized films upon film thickness and excitation wavelength

The observation of Raman signals even for thin oxidized films under

"non-SERS" conditions is suggestive of the presence of resonance Raman enhancement. This is also consistent with the strong absorption by these films throughout the visible region (5d,14) which yields a noticeable black coloration for thicker films. In order to distinguish clearly between contributions to the observed signals from surface and/or resonance Raman enhancement and to probe the role of light absorption as well as scattering within the film, we made systematic measurements of the intensity of the 480/560 cm^{-1} doublet as a function of film thickness and excitation wavelength.

Figure 5 shows a series of Raman spectra for oxidized nickel oxide layers of various film thicknesses; Figs. 5a-i refer to roughened gold substrates in 1 $\underline{M}$ KOH with 647.1 nm excitation (i.e. SERS conditions). The bottom spectrum (Fig. 5a) is for unmodified gold at 0.45 V. The broad band at 565 cm^{-1} is due to a gold-hydroxide stretch, as detailed in ref. 8d. The spectra in Figs. 5b-g show the effect of the presence of progressively increasing quantities of oxidized film, also at 0.45 V, with thicknesses denoted by the q_f values indicated. The intensity of the 480 and 560 cm^{-1} peaks first increases and then decreases with increasing film thickness, although the peak frequencies remain largely unchanged for films thicker than one monolayer.

These Raman bands for the thin films, say for $q_f^a \leq 2$ mC cm^{-2}, were found to be essentially depolarized, with a depolarization ratio $\rho \approx 0.7$, as commonly found for SERS (15). Significant polarization effects were observed, however, for the thicker films. For example, Figs. 5h and i show the spectra for a thick film ($q_f - 21$ mC cm^{-2}) on smooth gold using 647.1 nm excitation with the polarization vector perpendicular (Fig. 5h) and parallel (Fig. 5i) to the polarization plane of the incident light. These

data yield $\rho = 0.66$ and 0.21 for the 480 and 560 cm^{-1} bands, respectively. Similar depolarization ratios, 0.69 and 0.28, respectively, were obtained when using 514.5 nm excitation.

Plots of the combined integrated Raman intensities of the 480/560 cm^{-1} doublet as a function of film thickness, expressed as q_f, at gold using 647.1 nm excitation are given in Fig. 6. These data were obtained by depositing sequentially increasing quantities of nickel oxide on a given gold surface. The circles denote values obtained on roughened (SERS-active) gold while the squares are corresponding values for smooth (SERS-inactive) gold. While the former intensities reach a sharp maximum around $q_f^a \approx 1$ mC cm^{-2}, the latter increase monotonically with increasing thickness so that they approach the intensities obtained on roughened gold for $q_f \geq$ 15 mC cm^{-2}. Corresponding intensity-thickness plots using a smooth gold substrate irradiated with 488 nm light yielded curves that leveled off at significantly smaller thicknesses, corresponding to $q_f \geq 5$ mC cm^{-2}.

Given that the Raman signals from relatively thick films arise from bulk, rather than surface-enhanced, scattering mechanisms (vide infra), it is of interest to evaluate excitation profiles, i.e. the dependence of the integrated Raman intensity upon the laser excitation wavelength. Figure 7 shows a pair of such profiles for the 480 cm^{-1} (circles) and 560 cm^{-1} (squares) bands for a thick oxidized film on smooth gold, with a range of wavelengths between 457.9 to 676.4 nm. The Raman intensities were corrected for the wavelength dependence of the spectrometer throughput by means of Eq. [1]. The solid curve shown is the intensity-wavelength dependence (proportional to λ^{-4}) expected if normal Raman scattering predominates and the extent of light absorption by the film is negligible. (The statistical errors shown for the experimental points are averages

obtained from three independent measurements.) Instead of following this curve, however, the Raman intensities for both bands are seen to increase monotonically towards longer wavelengths.

DISCUSSION

Electrochemical Behavior

The present observation that the relatively thin $Ni(OH)_2$ films studied here are oxidized not to a trivalent state but effectively to $Ni^{3.7+}$ is consistent with previous findings for thicker films (5). This is also in harmony with the observation that $q_f/q_g > 0.5$ for $Ni(OH)_2$ deposition from $Ni(NO_3)_2$ solution, as follows. The observed specific role of NO_3^- anions is consistent with the following schematic mechanism (11b), whereby nitrate electroreduction releases OH^- ions that precipitate Ni^{2+} as $Ni(OH)_2$:

$$NO_3^- + 7H_2O + 8e^- \rightarrow NH_4^+ + 10OH^- \qquad [2a]$$

$$Ni^{2+} + 2OH^- \rightarrow Ni(OH)_2 \qquad [2b]$$

Although the products actually formed during NO_3^- electroreduction on gold are uncertain, Eq. [2] yields the largest number of OH^- ions, 1.25 per electron. If we then assume that the subsequent oxidation of the $Ni(OH)_2$ film requires only one electron (i.e. Ni^{3+} is formed), even if *all* the electrogenerated OH^- is consumed to produce precipitated $Ni(OH)_2$ the maximum q_f/q_g ratio predicted on this basis is 0.625. The observation of significantly larger q_f/q_g ratios therefore infers that the film can be oxidized beyond Ni^{3+}.

The deposition process from $Ni(ClO_4)_2$ or $NiSO_4$ solutions presumably utilizes OH^- released from H_2O reduction. This mechanism yields a maximum

predicted value of q_f/q_g equal to 0.5. The lower deposition efficiencies seen in Fig. 3 under these conditions may be due to the influence of H_2 bubbles that will be produced along with OH^- by H_2O reduction.

The similarity in the anodic-cathodic cyclic voltammograms for very thin (a few monolayers) and for thicker films is somewhat surprising (compare the solid and dotted traces in Fig. 2). The slight shift of the voltammetric peak potentials towards more positive values for the very thin films may well arise from the interaction with the gold substrate. Specific interactions between nickel hydroxide and substrates such as gold or platinum have been noted previously (16). The positive shift in the anodic peak potential brought about by potential cycling in basic solution has also been noted previously (5a, 11e, 17). This is believed to be due to the transformation of the disordered and hydrated form of precipitated $Ni(OH)_2$, termed "α-$Ni(OH)_2$", into a more crystalline "β-$Ni(OH)_2$" form (5c,17,18).

The negative drift of the open-circuit potential for the oxidized films, along with the disappearance of the corresponding surface Raman bands, can be rationalized by the occurrence of a spontaneous film discharge reaction leading to O_2 evolution. Such a process has been described previously (1b,5b). The related high electrocatalytic activity of the oxidized film for anodic O_2 formation may also account for the observation that $q_f^c < q_f^a$ at slow scan rates (cf. Fig. 2 and ref. 6). At higher scans the self-discharge process will be less important because of the shorter time scale involved.

Structural Interpretation of Raman Spectra

The SER spectra of thin $Ni(OH)_2$ films (Fig. 4a,b) is consistent with

the presence of α-Ni(OH)$_2$ given the similarity to the spectrum of freshly precipitated bulk-phase Ni(OH)$_2$ (Fig. 4c). The 455 cm^{-1} band is most likely due to a symmetric Ni-OH stretching mode (13a). This assignment is also consistent with the isotopic frequency ratio, $\nu(D_2O)/\nu(H_2O)$ = 0.98, observed for this band (6), since it is close to that predicted (0.972) for a symmetric M-OH vibration. The observation of a weak ill-defined band in the O-H stretching region for this material is also in harmony with the proposed structure for α-Ni(OH)$_2$ that features hydrogen-bound OH groups in a relatively hydrated and amorphous form (5c,17,18). The observation of a much more intense O-H stretch at 3580 cm^{-1} for the "aged" Ni(OH)$_2$ films in air, similar to commercial Ni(OH)$_2$ powder (Fig. 4d), is suggestive of the "β-Ni(OH)$_2$" form in which such hydrogen bonding is virtually absent (5c,18). The same conclusions have also been reached on the basis of infrared data (19).

A shift in the major Ni-OH stretching mode from ca. 460 to 445 cm^{-1} also appears to be characteristic of the transformation of α- to β-Ni(OH)$_2$ (compare Figs. 4c and d). The lack of significant changes in the Ni-OH as well as O-H stretch regions of the SER spectra (Fig. 4a,b) upon potential cycling or heating therefore suggests that these thin films remain primarily as α-Ni(OH)$_2$ in spite of the significant changes in their electrochemical redox properties under these conditions. This surprising result may arise from the likelihood that SERS senses predominantly the portion of the film molecularly close to the gold substrate. The structure of the first few monolayers may be significantly affected by its proximity to the metal surface.

The appearance of only the 480/560 cm^{-1} doublet characteristic of the oxidized film during the electrooxidation process indicates that no

important redox intermediates are formed en route to, or resulting from, attainment of the $Ni^{3.7}$ state. This would therefore appear to rule out formation of Ni^{3+} as part of a "heterogeneous" film containing, for example, domains of Ni(III) and Ni(IV) oxides.

The absence of a detectable deuterium isotope shift for the 480/560 cm^{-1} doublet indicates that at most only a small fraction (probably $\leq$ 20%) of the Ni-O bonds contributing to these modes involves hydroxide rather than oxygen groups. The absence of a detectable O-H stretching vibration for this film is also consistent with this finding. The relatively small depolarization ratio, 0.25, for the 560 cm^{-1} band together with its higher frequency is indicative of a symmetric O-Ni-O stretch, whereas the depolarized nature of the 480 cm^{-1} band indicates a mode of lower symmetry. From similar measurements on bulk samples, Jackovitz assigned the 560 and 480 cm^{-1} bands to a_{1g} Ni-O stretching and e_g Ni-O bending modes, respectively (13a).

These observations are largely consistent with the structure of the oxidized film proposed by Bode et al. (5c). The film stoichiometry can be written as $M(NiO_2)_3 \cdot xH_2O$ (x $\approx$ 2), where M is the metal countercation. Here the effective nickel "oxidation state" is 3.66 and only Ni-O rather than Ni-OH bonds are present, in accordance with the experimental observations. Although it is known that alkali metal cations can be incorporated into oxidized films (1a,5c,17) the absence of a significant influence upon the Ni-O vibrations indicates only weak cationic interactions.

Raman scattering mechanisms: film absorbance effects

The requirement of roughened gold surfaces and red (647.1 nm) laser excitation for the observation of Raman spectra for electrodeposited $Ni(OH)_2$ layers clearly diagnoses these signals as arising from SERS. The

difficulty of obtaining Raman signals even for very thick Ni(OH)$_2$ layers on substrates such as nickel, platinum or smooth gold, together with the observation of detectable signals on roughened gold down to submonolayer Ni(OH)$_2$ converages, attests to the magnitude of the surface enhancement (vide infra).

The observation of detectable, albeit weak, Raman signals for the oxidized film under "non-SERS" conditions (i.e. smooth gold and/or blue/green laser excitation) even for films only a few equivalent monolayers thick (e.g., Fig. 6) is indicative of the presence of extremely large Raman scattering cross sections. Given that the oxidized film exhibits strong electronic absorption throughout the visible region (5c,14) (cf dashed trace in Fig. 7) this enhancement is almost certainly due to a resonance Raman scattering mechanism. However, the much larger Raman signals observed for thin oxidized films on roughened gold (compare circles and squares in Fig. 6) are undoubtedly due to a surface-enhancement effect. Nevertheless, it is likely that electronic resonance as well as surface enhancement mechanisms contribute to these SERS signals; (i.e., so-called surface-enhanced resonance Raman scattering, SERRS, is operative) (20).

Surface enhancement factors (SEF) can be estimated roughly by comparing the spectral intensities for freshly prepared Ni(OH)$_2$ as presented in Fig. 4a (SERS, 647.1 nm) and Fig. 4c (normal Raman scattering, 488 nm). Even for the relatively thick samples (39 mg cm^{-2}), the optical absorbance of 488 nm can be neglected (5d). The ratios of Raman intensities, normalized for the different quantities of Ni(OH)$_2$ in the light beam and for different wavelengths employed yield SEF $\approx 4 \times 10^6$. Much lower surface enhancement factors, around 10^2, are obtained for oxidized films. These values can be obtained relatively directly from

Fig. 6 by comparing intensities for very thin films ($q_f^a \approx 0.5$ mC cm^{-2}) on roughened gold using 647.1 nm excitation with the corresponding Raman intensities on smooth gold. Surface-enhancement factors of ca. 10^6 are typical at silver for adsorbates not displaying electronic resonance enhancement in bulk (15,21); comparable values are also anticipated at gold in view of the similar SER intensities at these two metals (7a). It therefore appears that the extent of "electronic resonance" enhancement contained in the SERS of the oxidized film (i.e. SERRS) is substantially less than its contribution to the bulk-phase Raman intensities, so that the apparent SEF is correspondingly smaller.

The intriguing feature of Fig. 6 is that the Raman intensity-film thickness (I-d) dependencies are entirely different in the presence of SERS than in its absence. The sharply peaked dependence for SERS (circles) can be understood in terms of the thickness-dependent absorbance properties of the film, combined with the anticipated sharp decrease in the magnitude of the surface enhancement with increasing distance from the gold substrate. The scale of the latter dependence is unclear and may well depend upon the precise surface morphology (22). However, at least for electrochemically prepared surfaces, the intensity-distance dependence of SERS may well be sufficiently short range so that most of the observed signal arises from nickel-oxygen vibrations that are molecularly close (say within ca. 5-10Å) to the gold surface. In this case one expects the SERS I-d plot to yield a plateau for large d values. The observed gradual decrease in the Raman intensity for film thicknesses above ca. 5 equivalent monolayers (ca. 1 mC cm^{-2}) (Fig. 6) can then be explained readily by the decreasing penetration of the incoming light to (and back-scattered light from) the SERS sites on the inner "edge" of the layer as a result of the high absorptivity of the

oxidized film.

The markedly different form of the I-d profile in the absence of SERS (squares, Fig. 6) is also consistent with the effect of film absorbance. Resonance Raman scattering (RRS) should take place throughout the film, so that I increases linearly with d. However, for sufficiently thick layers so that the effective light penetration depth is smaller than the film thickness I will become independent of d, as is observed (Fig. 6). Since RRS should contribute similarly to the I-d profiles for the SERS-active as for the SERS-inactive surfaces, the difference between these two curves should yield the intensity-thickness profile, I_{SER} - d, associated with SERS alone. This difference is denoted by the dashed trace in Fig. 6.

It is of interest to ascertain if the I_{SER} - d profile is also quantitatively in accordance with the known optical absorbance properties of the nickel oxide film (14). On the basis of the above model, we expect that the decreases in I_{SER} with increasing d arise from light absorption within the film and therefore should be related closely to the normalized reflectivity changes, $\Delta R/R_o$, observed in an absorption-reflection experiment. The linearized $\Delta R/R_o$ values for s- and p-polarized light are given by Eqs. 3a and b, respectively (23):

$$(\Delta R/R_o)_s = \frac{8\pi d n_1 \cos\phi_1}{\lambda} \cdot \mathrm{Im} \left(\frac{\hat{\epsilon}_2 - \hat{\epsilon}_3}{\epsilon_1 - \hat{\epsilon}_3} \right) \qquad [3a]$$

$$(\Delta R/R_o)_p = \frac{8\pi d n_1 \cos\phi_1}{\lambda} \cdot \mathrm{Im} \left(\frac{\hat{\epsilon}_2 - \hat{\epsilon}_3}{\epsilon_1 - \hat{\epsilon}_3} \cdot \frac{\hat{\epsilon}_2\hat{\epsilon}_3 - \epsilon_1(\hat{\epsilon}_2 + \hat{\epsilon}_3)\sin^2\phi_1}{\hat{\epsilon}_2\hat{\epsilon}_3 - \hat{\epsilon}_2(\epsilon_1 + \hat{\epsilon}_3)\sin^2\phi_1} \right) \qquad [3b]$$

where R_o is the reflectivity of gold, d the film thickness, n_1 the refraction index of the electrolyte, λ the wavelength, ϕ_1 the incident

angle versus the surface normal, and Im designates the imaginary part of the following expressions, where $\hat{\epsilon}_i$ are the complex dielectric constants $(\hat{\epsilon}_i = \epsilon_i' - \epsilon_i'')$ for the electrolyte $(\epsilon_1 = n_1^2)$, nickel oxide $(\hat{\epsilon}_2)$ and gold $(\hat{\epsilon}_3)$.

In our experiment, ϕ_1, λ, and the polarization of the incident and scattered light are not the same. For our optical geometry (illustrated in the insert of Fig. 6) and given that $n_1 = 1.35$ and $n_{glass} \approx 1.52$ we obtain $\phi_1 = 40°$. The corresponding average angle for the scattered beam is $22°$, since light is collected over a cone which is determined by the size and position of the focusing lens. As a first approximation we therefore take average values and set $\phi_1 = 30°$ and $\lambda = 660$ nm, the latter being midway between the wavelengths of the incident and scattered light. The required values of the dielectric constants at this wavelength are: for the oxidized film, $\hat{\epsilon}_2 = 8.6 - 8.6\,i$, (14); and for gold $\hat{\epsilon}_3 = -13.2 - 0.9\,i$, (24). Thus we obtain the following thickness-dependent $\Delta R/R_o$ values:

$$(\Delta R/R_o)_s = 2.7 \times 10^5 \; d/cm \qquad [4a]$$

$$(\Delta R/R_o)_p = 3.6 \times 10^5 \; d/cm \qquad [4b]$$

Since the incident light employed in our experiment was s-polarized, and that the scattered light is largely depolarized we anticipate that the effective $\Delta R/R_o$ value for our purpose will be intermediate between that given by Eqs. [4a] and [4b]. This can be related directly to the slope of the initial decay of I_{SER} with d, expressed as $\Delta I_{SER}/I_{SER}^o$, where I_{SER}^o is the SERS intensity extrapolated to zero film thickness. From Fig. 6, this slope (dotted line), is equal to $0.2\ q_f$ (mC cm^{-2}). It is necessary, however, to convert the q_f values plotted in Fig. 6 to a thickness scale.

In order to be consistent with the above $\Delta R/R_o$ estimate, we need to perform this conversion in the same fashion as in ref. 14. Presuming that this was based on a one-electron oxidation and an average Ni-Ni distance of 3.4Å, we obtain the approximate result:

$$\Delta I_{SER}/I^\circ_{SER} - 8 \times 10^5 \; d/cm \tag{5}$$

Thus the optical absorbance of the oxidized film is somewhat higher than in Eq. [4]. This difference most likely reflects the relatively crude approximations involved, such as the assumption that the reflectivity for roughened and smooth gold are identical and the neglect of interactions between the gold surface and the very thin oxidized films employed here. Nevertheless, we deduce that the thickness dependence of the Raman signals under conditions where SERS (or SERRS) as well as where RRS mechanisms predominate can be accounted for at least semi-quantitatively by including the influence of absorption of the incident, reflected, and scattered light within the film.

The effect of altering the laser wavelength upon the Raman intensity under conditions where RRS dominates, as in Fig. 7, can also be rationalized at least qualitatively in terms of film absorption effects. Thus the marked increase of the Raman intensity towards longer wavelengths corresponds to a monotonic decrease in the film absorbance under these conditions (Fig. 7). Increasing the wavelength will increase the penetration depth of the light into the relatively thick (~ 100 monolayers) film, thereby increasing the intensity of the Raman scattered light.

21

Concluding Remarks

We believe that the present results demonstrate the combined virtues of surface-enhanced Raman scattering and resonance Raman scattering for obtaining in-situ structural information for thin metal oxide films on gold electrodes. Thus the SERS probe enables vibrational information to be obtained for various redox states for thin films irrespective of their electronic absorption properties. At least for redox states displaying suitable electronic characteristics, resonance Raman spectroscopy can provide valuable additional characterization. The SERS and RRS probes are complementary in that they tend to probe the inner and outer regions of the film, respectively.

This suggests, for example, that useful spatial information on the dynamics of film redox conversions might be obtained from time-resolved Raman spectral measurements under transient electrochemical conditions. Such measurements for several different metal oxide films on gold electrodes are underway in this laboratory (25).

ACKNOWLEDGMENTS

REFERENCES

1. a) G. W. D. Briggs, in "Specialist Periodical Reports-Electrochemistry", Vol. 4, H. R. Thirsk, ed., Chemical Society, London, 1974, Chapter 3; b) P. C. Milner and U. B. Thomas, "Advances in Electrochemistry and Electrochemical Engineering", Vol. 5, C. W. Tobias, ed., Interscience, New York, 1967, p. 1; c) G. Halpert, J. Power Sources, 12, 177 (1984).

2. a) M. Fleischmann, K. Korinek, and D. Pletcher, J. Chem. Soc. Perkin II, 1972, 1396; b) J. Kaulen and H. J. Schäfer, Tetrahedron, 38, 3299 (1982); c) P. M. Robertson, P. Berg, H. Reimann, K. Schleich, and P. Seiler, J. Electrochem. Soc., 130, 591 (1983); d) D. E. Hall, J. Electrochem. Soc., 132, 41C (1985).

3. C. M. Lampert, Solar Energy Mat., 11, 1 (1984).

4. a) J. L. Ord, Surf. Sci., 56, 413 (1976); b) R. S. Schrebler Guzman, J. R. Vilche, and A. J. Arvia, J. Electrochem. Soc., 125, 1578 (1978); c) R. E. Carbonio, V. A. Macagno, M. C. Giordano, J. R. Vilche, and A. J. Arvia, J. Electrochem. Soc., 129, 983 (1982); d) B. Beden, D. Floner, J. M. Léger, and C. Lamy, Surf. Sci., 162, 822 (1985).

5. a) P. Oliva, J. Leonardi, J. F. Laurent, C. Delmas, J. J. Braconnier, M. Figlarz, F. Fievet, and A. de Guibert, J. Power Sources, 8, 229 (1982); b) B. E. Conway and M. A. Sattar, J. Electroanal. Chem., 19, 351 (1968); c) H. Bode, K. Dehmelt, and J. White, Z. Anorg. Allg. Chem., 366, 1 (1969) d) D. A. Corrigan and S. L. Knight, Electrochemical Society, Extended Abstracts. Vol. 86-2, San Diego, CA, October 1986.

6. J. Desilvestro, D. A. Corrigan, and M. J. Weaver, J. Phys. Chem., in press.

7. a) P. Gao, M. L. Patterson, M. A. Tadayyoni, and M. J. Weaver, Langmuir, 1, 173 (1985); b) P. Gao and M. J. Weaver, J. Phys Chem., 89, 5040 (1985); c) M. L. Patterson and M. J. Weaver, J. Phys. Chem., 89, 5046 (1985); d) P. Gao and M. J. Weaver, J. Phys. Chem., 90, 4057 (1986).

8. a) M. A. Tadayyoni, P. Gao, and M. J. Weaver, J. Electroanal. Chem., 198, 125 (1986); b) M. A. Tadayyoni and M. J. Weaver, Langmuir, 2, 179 (1986); c) M. J. Weaver, P. Gao, D. Gosztola, M. L. Patterson, and M. A. Tadayyoni, ACS Symp. Ser., 307, 135 (1986); d) J. Desilvestro and M. J. Weaver, J. Electroanal. Chem., 209, 377 (1986).

9. a) L-W. H. Leung and M. J. Weaver, J. Electroanal. Chem., in press; b) L-W. H. Leung and M. J. Weaver, in preparation; c) D. Gosztola, unpublished results.

10. M. A. Tadayyoni, S. Farquharson, T. T-T. Li, and M. J. Weaver, J. Phys. Chem., 88, 4701 (1984).

11. a) H. K. Embaby and A. A. Moussa, J. Chem. Soc., 1958, 4027; b) E. Häusler, in "Power Sources", D. H. Collins, ed., Pergamon, Oxford, 1966, p. 287; c) D. M. MacArthur, in "Power Sources", D. M. Collins, ed., Vol. 3, Oriel Press, Newcastle-upon-Tyne, 1971, p. 91; d) T. Takamura, T. Shigorami, and T. Nakamura, Denki Kagaku, 42, 582 (1974); e) W. Visscher and E. Barendrecht, J. Electroanal. Chem., 154, 69 (1983).

12. R. K. Chang and B. L. Laube, CRC Crit. Rev. in Solid State Mat. Sci., 12, 1 (1984).

13. a) J. F. Jackovitz, in "Proc. Symp. on the Nickel Electrode", R. G. Gunther, S. Gross, eds., Electrochemical Society, Pennington, NJ, 1982, p. 48. b) C. A. Melendres and S. Xi, J. Electrochem. Soc., 131, 2239 (1984).

14. J. D. E. McIntyre and D. M. Kolb, Symp. Far. Soc., 4, 99 (1970).

15. For example, R. P. Van Duyne in "Chemical and Biochemical Applications of Lasers", Vol. 4, C. B. Moore, ed., Academic Press, New York, 1979, p. 101.

16. a) V. A. Macagno, J. R. Vilche, and A. J. Arvia, J. Electrochem. Soc., 129, 301 (1982); b) M. E. Folquer, J. R. Vilche, and A. J. Arvia, J. Electrochem. Soc., 127, 2634 (1980).

17. R. Barnard, C. F. Randell, and F. L. Tye, J. Appl. Electrochem., 10, 109, 127 (1980).

18. a) G. W. D. Briggs and W. F. K. Wynne-Jones, Electrochim. Acta, 7, 241 (1962); b) H. Bode, K. Dehmelt, and J. Witte, Electrochim. Acta, 11, 1079 (1966); c) R. S. McEwen, J. Phys. Chem., 75, 1782 (1971).

19. a) F. Kober, J. Electrochem. Soc., 112, 1064 (1965); b) M. Figlarz and S. Le Bihan, C. R. Acad. Sc. Paris, 272, 580 (1971).

20. For example, R. P. Van Duyne and J. P. Haushalter, J. Phys. Chem., 89, 2999 (1983).

21. M. J. Weaver, S. Farquharson, and M. A. Tadayyoni, J. Chem. Phys. 82, 4867 (1985).

22. M. Moskovits, Rev. Mod. Phys., 57, 783 (1985).

23. J. D. E. McIntyre, in "Advances in Electrochemistry and Electrochemical Engineering", Vol. 9, R. H. Muller, ed., Wiley, New York, 1973, p. 61.

24. D. M. Kolb and J. D. E. McIntyre, Surf. Sci., 28, 321 (1971).

25. D. Gosztola, unpublished experiments.

Figure Captions

Fig. 1

Potential-time curves for galvanostatic deposition of $Ni(OH)_2$ from quiescent 0.01 $\underline{M}$ Ni(II) solutions, with a cathodic current density of 0.8 mA cm^{-2}, and following open-circuit decay curves. Solid traces: deposition on electrochemically roughened gold from $Ni(NO_3)_2$, $Ni(ClO_4)_2$, or $NiSO_4$ solutions as indicated. Dashed trace: deposition on roughened gold from 0.01 $\underline{M}$ $Ni(ClO_4)_2$/0.005 $\underline{M}$ KNO_3.

Fig. 2

Anodic-cathodic cyclic voltammograms for $Ni(OH)_2$ deposited on electrochemically roughened gold in 1 $\underline{M}$ KOH. The scan rate was 2 mV s^{-1}. $Ni(OH)_2$ was deposited ex situ from 0.01 $\underline{M}$ $Ni(NO_3)_2$ solution with a constant cathodic current density of 0.8 mA cm^{-2} for 3.0 s (solid and dashed traces) or 60 s (dotted curve). The initial scans are shown by the solid and dotted traces. Dashed trace is voltammogram obtained after 150 cycles between -0.1 and 0.45 V at a scan rate of 50 mV s^{-1}.

Fig. 3

Faradaic charge density q_f for film oxidation as a function of cathodic charge density q_g passed during galvanostatic deposition of $Ni(OH)_2$. q_f was determined by integrating the anodic voltammetric waves (as in Fig. 2). $Ni(OH)_2$ films were deposited on electrochemically roughened gold electrodes form 0.01 $\underline{M}$ $Ni(NO_3)_2$ (circles), 0.01 $\underline{M}$ $Ni(ClO_4)_2$ (squares), and 0.01 $\underline{M}$ $NiSO_4$ (triangles). The solid lines represent q_f/q_g - 1 and 0.5, respectively.

Fig. 4

Surface-enhanced Raman (a,b) and normal Raman spectra (c,d) of $Ni(OH)_2$.
Thin $Ni(OH)_2$ film (q_f - 1.1 mC cm^{-2}) on electrochemically roughened gold
(a) in air and (b) in 1 $\underline{M}$ KOH at E - -0.2 V with λ_{ex} - 647.1 nm. (c) 15 mg
$Ni(OH)_2$ powder, obtained from cathodically induced precipitation on Ni,
washing, and drying in air, mixed and pressed with 45 mg KBr to a pellet,
and rotated while recording Raman spectra (λ_{ex} - 488.0 nm) (d)
Commercially obtained β-$Ni(OH)_2$ powder, same conditions as for (c). The
laser intensity at all samples was 60 mW, with the exception of 20 mW for
the 3300-3750 cm^{-1} region in (d).

Fig. 5

Raman spectra for oxidized nickel oxide films, under various conditions
corresponding to q_f values between 0.0 (a) and 13.5 mC cm^{-2} (g), as
indicated, were deposited on electrochemically roughened gold and oxidized
in situ in 1 $\underline{M}$ KOH at E - 0.45 V. Laser excitation was 647.1 nm, 60 mW at
the sample. Spectra (b)-(g) were obtained from the same roughened
electrode by sequentially depositing $Ni(OH)_2$ ex situ, recording Raman
spectra at 0.45 V, dissolving the reduced film in 0.1 $\underline{M}$ $HClO_4$ for 30 min.,
and rinsing with water. (h,i) Nickel oxide layer (q_f - 21 mC cm^{-2}) on
smooth gold in 1 $\underline{M}$ KOH at E - 0.45 V, with scattered light polarized
perpendicular ($I_\perp$) and parallel ($I_\parallel$) with respect to the incident light
(λ_{ex} - 647.1 nm, 135 mW at the sample). Dotted traces indicate the
baselines used for the integration over the 480 and 560 cm^{-1} bands. (j)
Raman spectrum of an ex situ oxidized $Ni(OH)_2$ film on smooth gold (q_f - 18
mC cm^{-2}) measured in air. λ_{ex} - 514.5 nm, 100 mW at the sample. The
reduction of the oxidized nickel oxide under open-circuit conditions did

not alter the spectra of these "thick" films during data acquisition.

Fig. 6

Integrated Raman intensities (350-700 cm^{-1}, arbitrary units) on electrochemically roughened (circles) and smooth (squares) gold electrodes as a function of oxidized film thickness, as denoted by voltammetric q_f values. Electrolyte is $1\underline{M}$ KOH, E - 0.45 V, λ_{ex} - 647.1 nm, 60 mW at the sample. The dashed curve is the difference between the two solid lines that are drawn through the experimental points. Insert: schematic of cell and electrode arrangement; arrows indicate the direction of the incident and scattered light.

Fig. 7

Excitation profiles for oxidized nickel oxide (q_f - 21 mC cm^{-2}) on smooth gold in 1 $\underline{M}$ KOH for E - 0.45 V, shown as integrated Raman intensities for the 480 cm^{-1} (circles) and the 560 cm^{-1} band (squares) as a function of excitation wavelength. The Raman intensities were normalized for spectrometer throughput and photomultiplier response with respect to λ_{ex} - 457.9 nm according to Eq. [1]. The error bars represent the standard deviations obtained from 3 experimental runs. The solid trace represents the relative Raman intensities expected for normal Raman scattering of a colorless sample. The dashed curve is the absorption spectrum of oxidized nickel oxide film corresponding to q_f - 19 mC cm^{-2} on an optically transparent gold/quartz substrate (cf. ref. 5d).
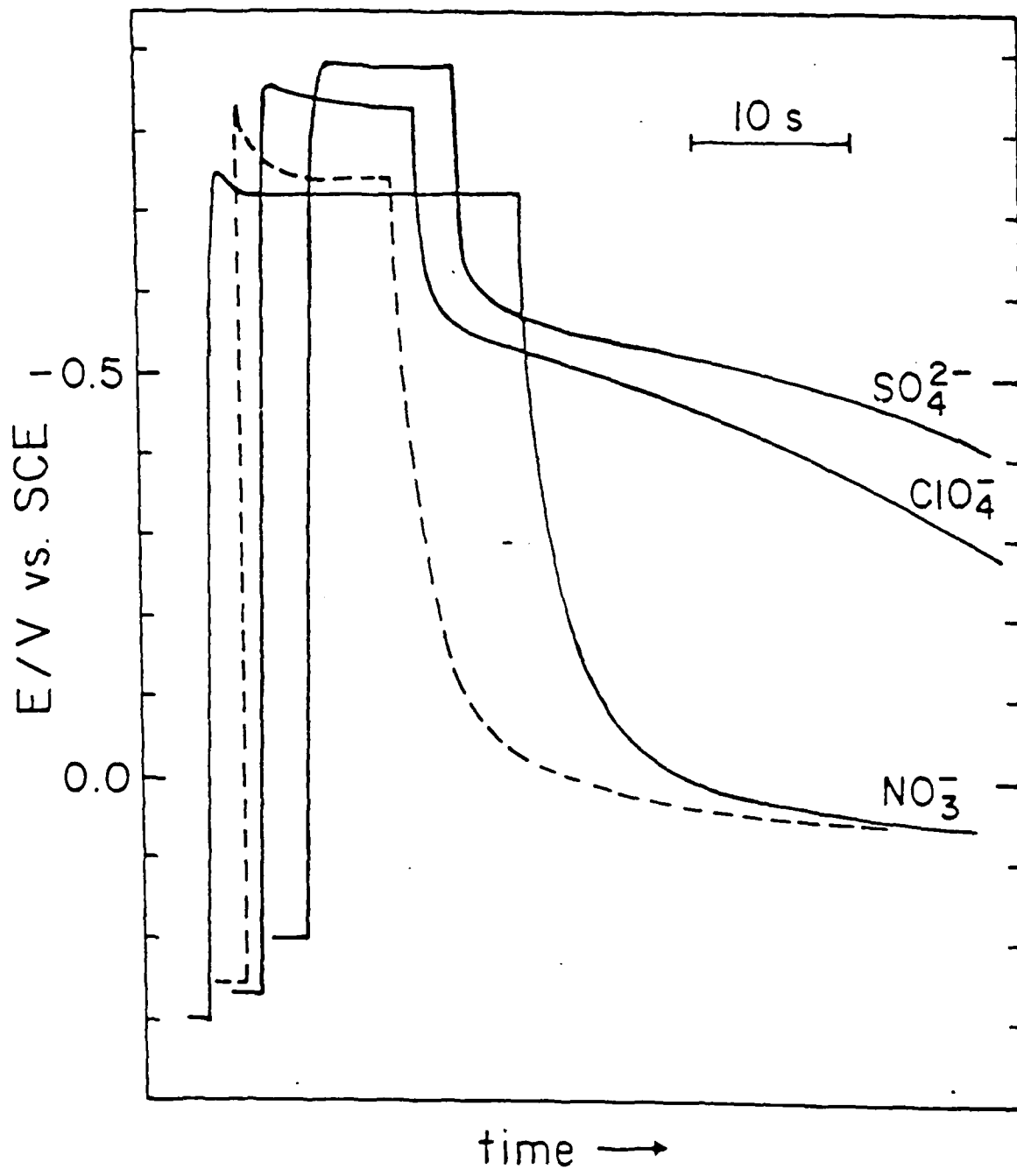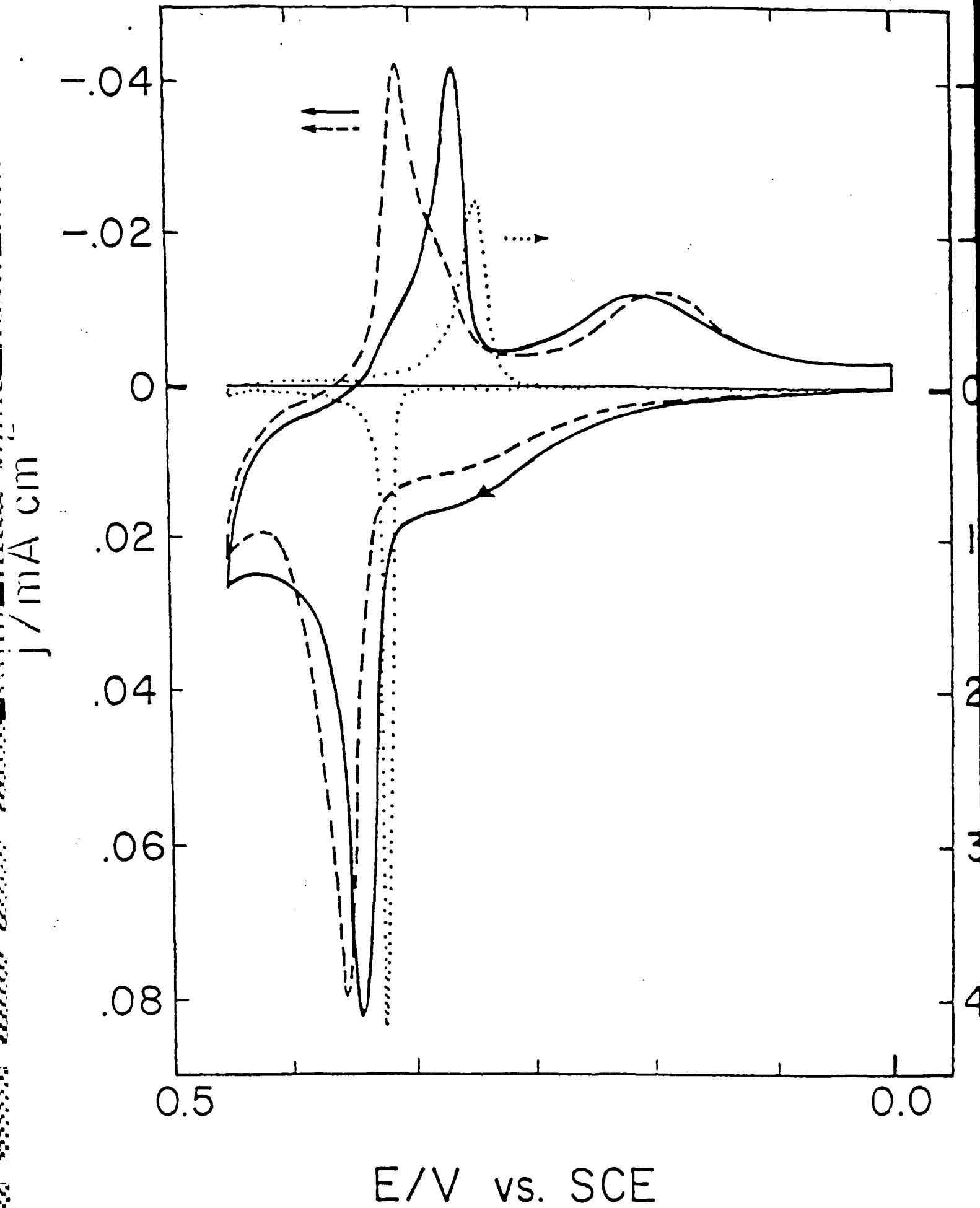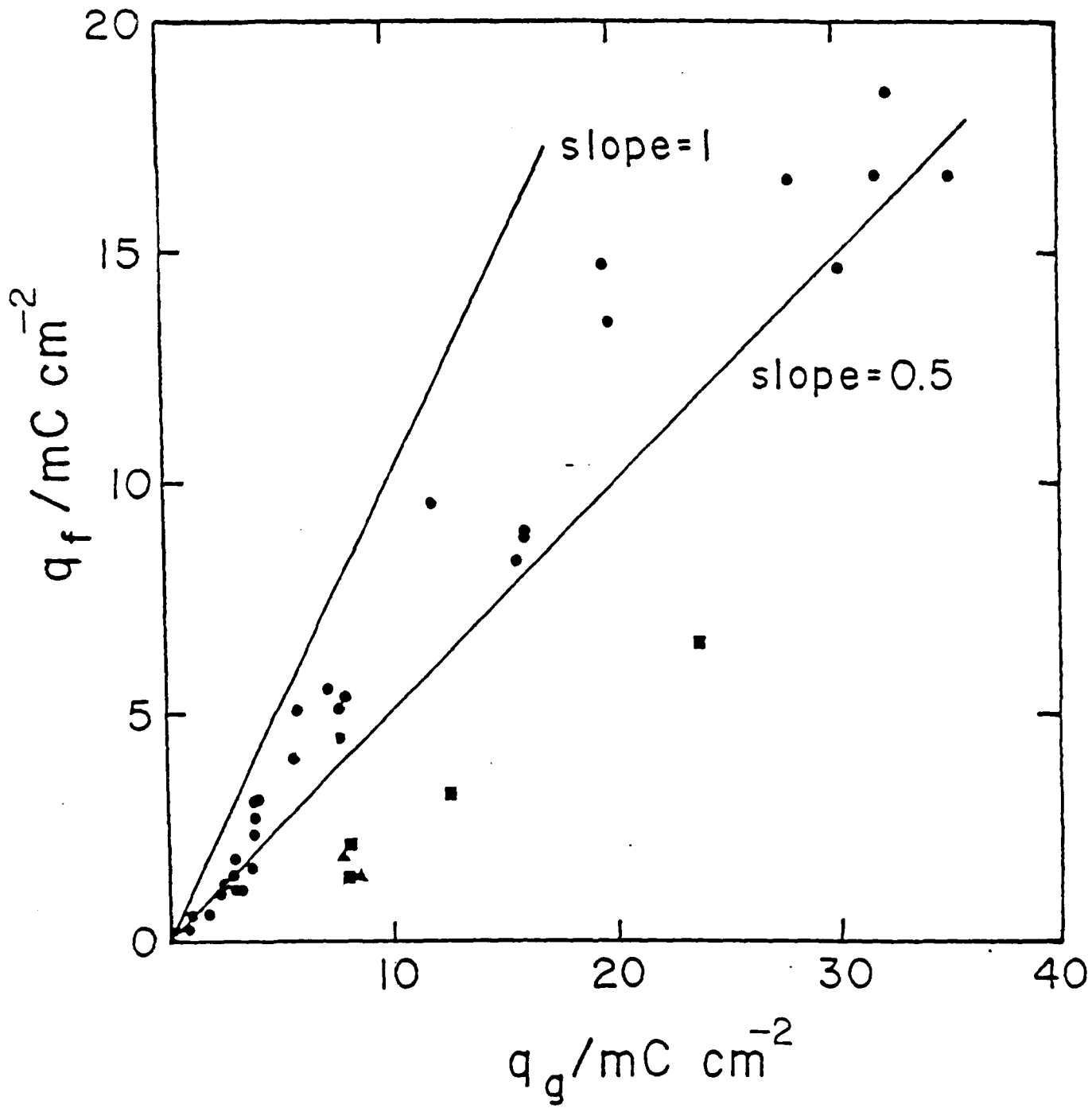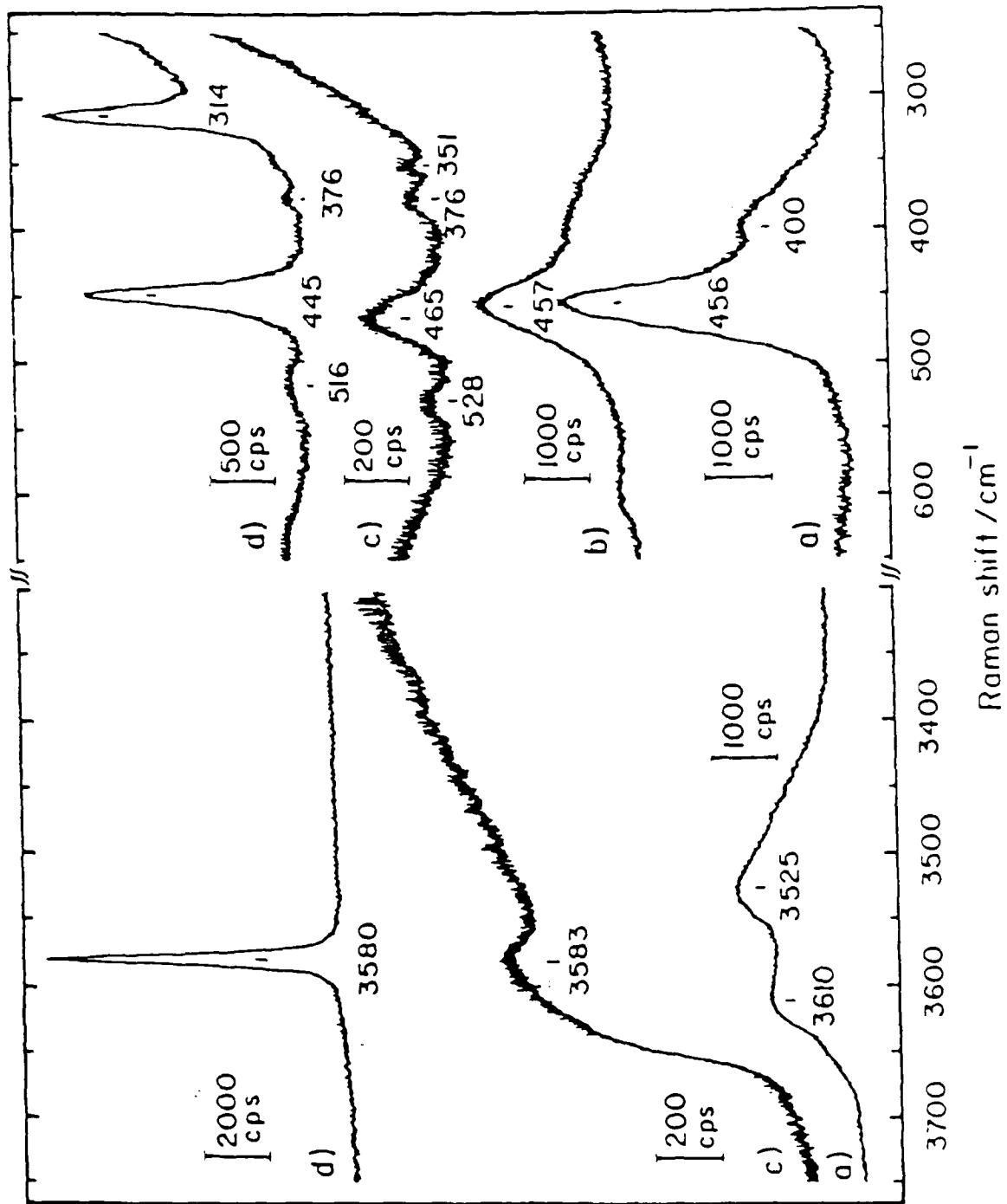
Fig. 1

Fig. 4

Raman shift /cm⁻¹

314
376
445
516
d) 500 cps

351
376
465
528
c) 200 cps

457
b) 1000 cps

400
456
a) 1000 cps

3580
d) 2000 cps

3583
3525
3610
c) 200 cps
a)
1000 cps

200 cps

560

479

j)

$I_{||}$

i)

$I_{\perp}$

50 cps

h)

g)

qf = 13.5 mC cm^{-2}

1000 cps

f)

4.1

e)

2.4

559

481

d)

1.3

c)

0.14

1000 cps

561

485

b)

0.03

564

a)

0.0

700   600   500   400

Raman shift /cm^{-1}
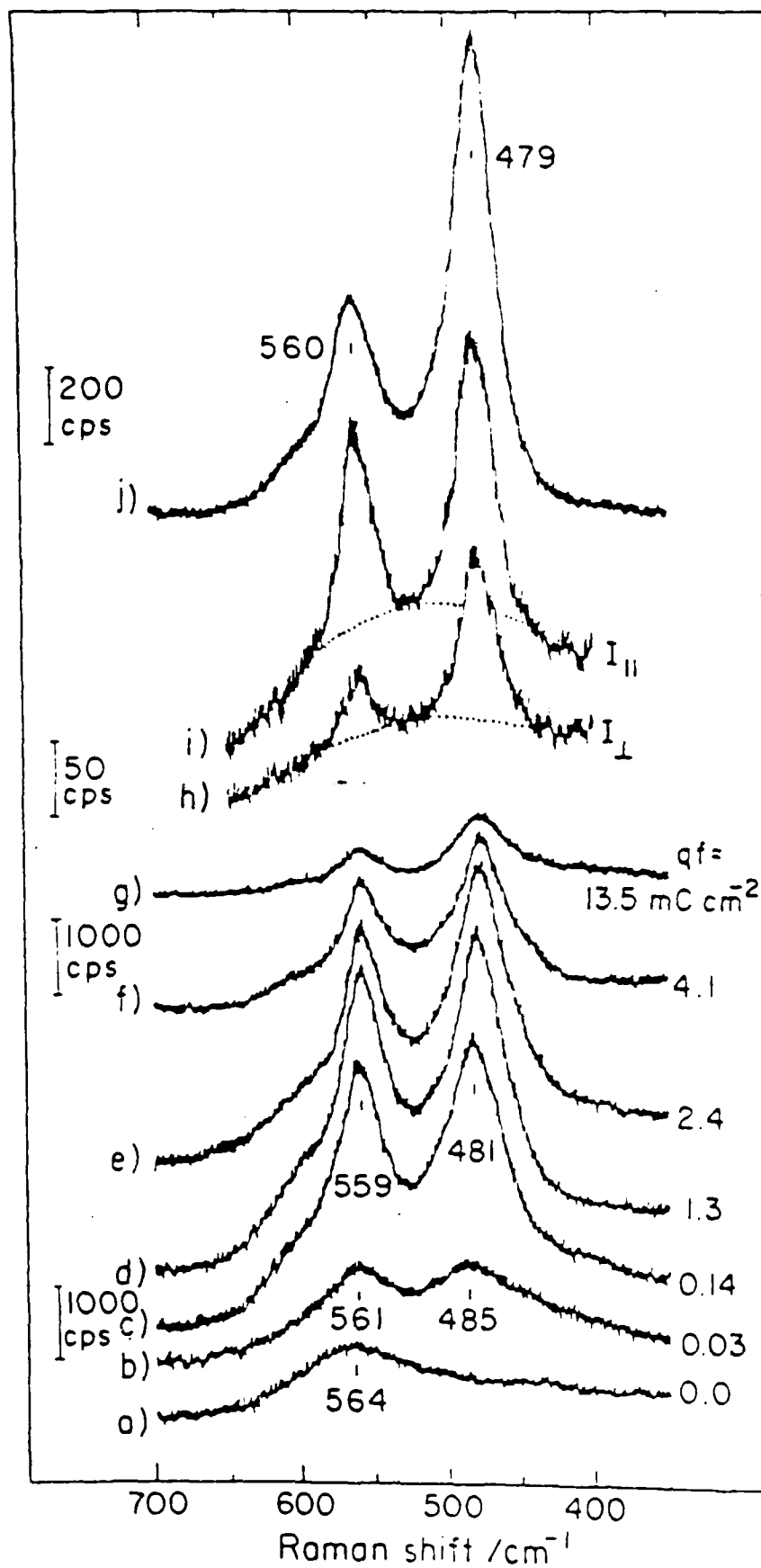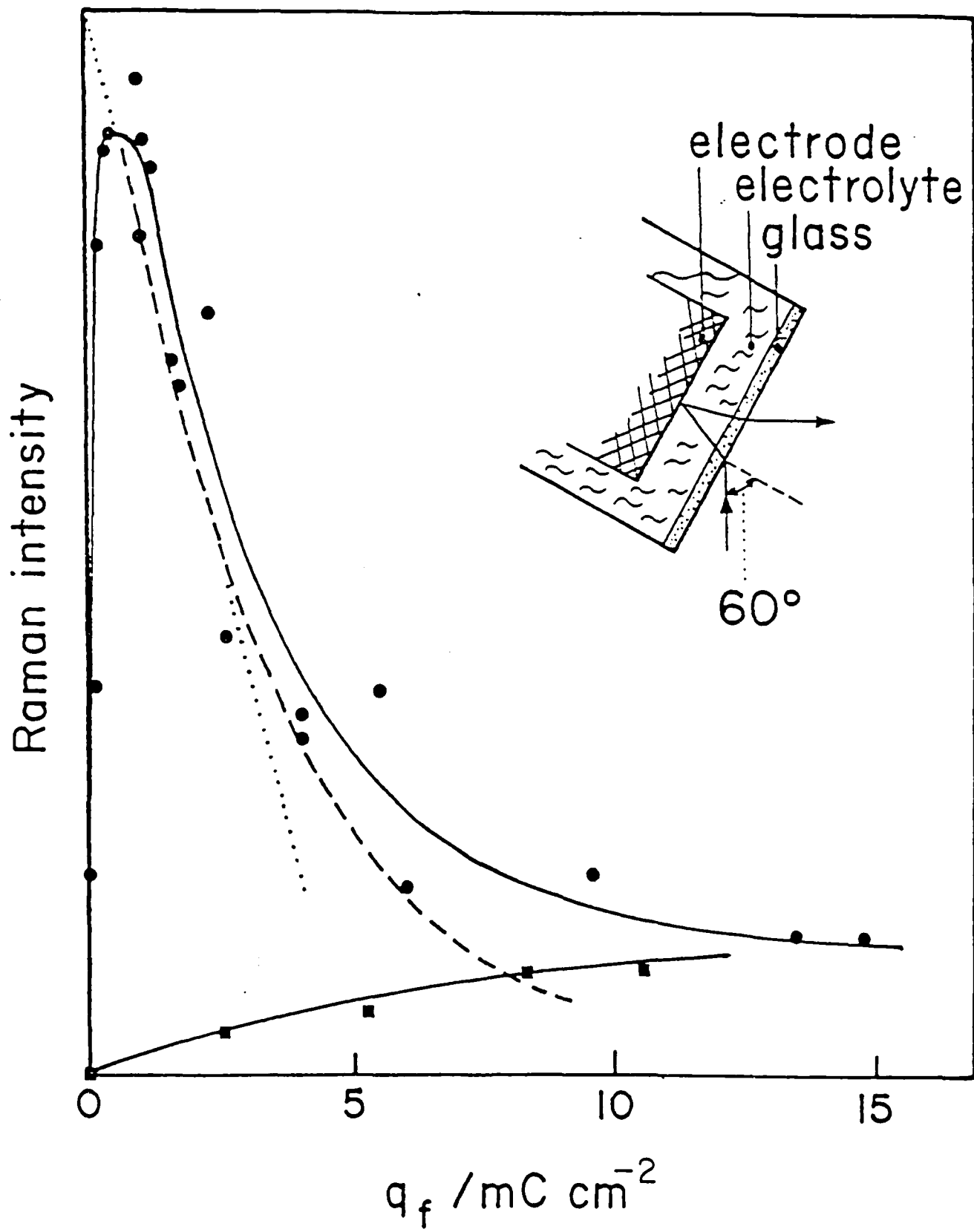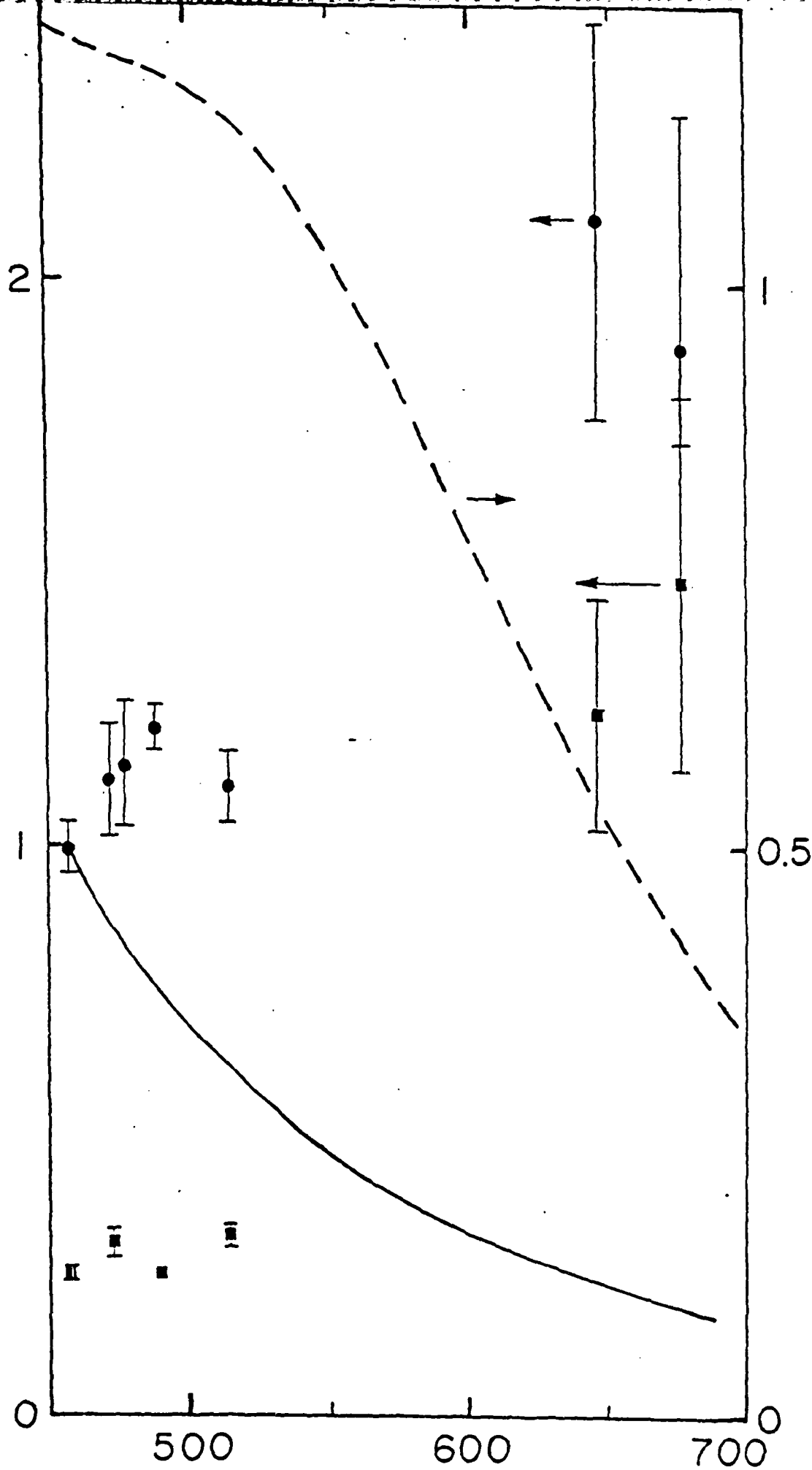
END

DATE

FILMED

MARCH

1988

DTIC